Direct FEM-Domain Decomposition using Convex-to-Concave Spherical Ports for Space Applications

Pedro Robustillo, Jesus Rubio, Juan Zapata, and Juan R. Mosig, *Life Fellow, IEEE*

***Abstract*— This paper proposes the application of a hybrid numerical technique to two cases of interest in the space business: the reallocation of radiators and scatters on satellite platforms; and the analysis of antennas for mobile communications. It is based on the analytical manipulation of the Generalized Scattering Matrix obtained from the Finite Element Method, when concave and convex spherical surfaces are defined as ports. The technique combines the power of full-wave resolution, the flexibility and speed of the Direct Domain Decomposition techniques, and the application of analytical rotations and translations from the addition theorems for spherical vector waves while keeping the same accuracy as a complete full-wave method since no model simplifications are considered.**

***Index Terms*— Spherical modes port, satellite applications, lens antenna, finite element method, Ka-band.**

I. Introduction

As known from the basics of electromagnetics, two or more bodies that are close to each other in terms of wave-length generate a global electromagnetic (EM) behavior that depends on both the sum of the effect generated by each body independently, and their mutual interactions.

This situation is ubiquitous in applications related to space. Focusing on the space segment, satellites are complex structures involving several EM-sensitive bodies whose study requires a multiphysics approach (mechanical, thermal, electrical, etc.). In addition, the geometry of new satellite platforms is often prone to changes during its design cycle [1]. Therefore, reallocation of scatters and antennas is a frequent need. This process may require a full EM analysis of the new structure each time a change is introduced, turning into a very consuming process; and/or the use of simplified models.

On the ground segment, dielectric lens antennas have been proposed during the last years for Ka-band communications on the move [2]. Among their virtues, they offer high gain and their manufacturing process is well controlled. The lens design is usually carried out according to asymptotic methods (AM) which, in general, provide the lens shape and profile needed to meet the specifications. But the interactions between lens and feeder are not taken into account and this frequently results in a poor prediction of the lens performances. Furthermore, for communications on the move, the lens may move with respect to the feeder to obtain beam steering, so a complete full-wave analysis would be needed for each steering angle.

The idea of Domain Decomposition (DD) has already been proposed in the literature [3-5]. In [4], the location of an antenna on an airplane fuselage is presented. And in [5], the use of AM plus spherical mode expansion is used to obtain the modifications in the feeder's S_{11} parameter.

In this work, DD is fully incorporated into a hybrid technique based on the Finite Element Method (FEM) combined with mathematically-accurate analytical matrix manipulations. The main goal is to develop a technique allowing placing, reallocations, and rotations of antennas and scatters on or near a bigger domain (such as a satellite fuselage or a lens), so that the EM impact of each modification can be quickly obtained with a very reduced computational effort, while offering an *exact* solution of the complete problem. As it will be shown, this novel technique relays on the proper combination of the FEM-computed Generalized Admittance Matrix (GAM) for each domain of interest ([3], [6]), and the well-known spherical mode expansions to model the free-space between a convex spherical port (CxSp, being the outer boundary of a domain) and a concave spherical port (CvSp, being the "host" port in a bigger domain). These spherical ports are allowed to have arbitrary centers and radii. This hybrid technique will be fully described in Section II, while Section III contains the obtained results from the two relevant cases highlighted in this Introduction: beam-steerable lens antenna and antenna reconfiguration on sat-platforms.

II. Direct DD Based on Spherical Ports

A. Step-by-step description

The technique proposed can be broken-down as follows:

1) Solving the FEM problems, including CxSp and CvSp. There will be a number of smaller domains, D_i, each of them with (at least) a CxSp as outermost boundary, generating each a GAM_i; and a bigger domain, D_H, with, at least, a CvSp (that will host domains D_i) yielding GAM_H.

This paper was submitted for review in May, 2020. This work was partially supported by FEDER (European Union), Ministerio de Economía y Competitividad (Spanish Government) and Junta de Extremadura under projects TEC2017-83352-C2-2-P and GR18055.

P. Robustillo was with LEMA-EPFL (see below). He is now with AIRBUS, Friedrichshafen, Germany (e-mail: pedro.robustillo@airbus.com).

J. Rubio is with Escuela Politécnica, Universidad de Extremadura, Cáceres, Spain (e-mail: jesusrubio@unex.es).

J. Zapata was with ETSIT, Universidad Politécnica de Madrid, Madrid, Spain (e-mail: jzapata@etc.upm.es).

J. R. Mosig was with the Laboratory of Electromagnetism and Antenna at Ecole Polytechnique Fédérale de Lausanne (LEMA-EPFL), Lausanne, Switzerland (e-mail: juan.mosig@epfl.ch).

2) Obtaining the Generalized Scattering Matrix, GSM_i, associated to each GAM_i. Described in Section II.B.

3) Applying the traslation/rotation theorems to all GSM_is, yielding the analytically-built GSM_G. This operation accounts for all the couplings between the GSM_is, explained in [6-7].

4) Relating the several CxSps of the GSM_G to a single CxSp which will fit into the CvSp of D_H, by using the procedure explained in Section II.C, yielding GSM_C. This CxSp must enclose all the CxSps of the many GSM_is.

5) Converting the GSM_C into GAM_C.

6) Perform the connection of GAM_C and GAM_H, yielding the GAM of the complete problem, say GAM_T.

B. Conversion from GAM to GSM and viceversa

In the frame of this work, it was found that connection of a GSM-CxSp to a GSM-CvSp laid to issues with interpretation and convergence in relation to CvSp. On the other hand, connection of a GAM-CxSp to a GAM-CvSp was successfully checked, as will be shown. However, GSMs for regions with convex ports need to be calculated since they provide the reflection and radiation characteristics of the device, and they allow using analytical tools to account for rotations, changing the origin of the spherical modes, and computing mutual couplings.

The GSM, denoted as $\boldsymbol{S}$, of the device is obtained from the GAM through the expressions that relate complex amplitudes of voltages and currents with: complex amplitudes of incident (v_l^+) and reflected modes (v_l^-) in plane ports (WGp); and incoming (a_{im}) and outgoing (b_{im}) spherical modes in spherical ports. These relations are well known for plane ports. For spherical ports they are given through the Schelkunoff Spherical Hankel functions of first and second kind [8]. In a general way, we express it as:

$$\begin{aligned} V_{im} &= a_{im}A_{im} + b_{im}B_{im} \\ I_{im} &= a_{im}C_{im} + b_{im}D_{im} \end{aligned} \tag{1}$$

which leads to the following relation between the GSM and the GAM, $\boldsymbol{Y}$:

$$\boldsymbol{S} = (\boldsymbol{YB} - \boldsymbol{D})^{-1}(\boldsymbol{C} - \boldsymbol{DB}^{-1}\boldsymbol{A}) - \boldsymbol{B}^{-1}\boldsymbol{A} \tag{2}$$

where $\boldsymbol{A}$, $\boldsymbol{B}$, $\boldsymbol{C}$ and $\boldsymbol{D}$ are diagonal matrices whose elements are computed from the aforementioned spherical modes, and with $\boldsymbol{S}$ defined as

$$\boldsymbol{S}\begin{bmatrix}\boldsymbol{v}^+\\ \boldsymbol{a}\end{bmatrix} = \begin{bmatrix}\boldsymbol{\rho} & \boldsymbol{r}\\ \boldsymbol{t} & \boldsymbol{s}\end{bmatrix}\begin{bmatrix}\boldsymbol{v}^+\\ \boldsymbol{a}\end{bmatrix} = \begin{bmatrix}\boldsymbol{v}^-\\ \boldsymbol{b}\end{bmatrix} \tag{3}$$

where $\boldsymbol{v}^+$, $\boldsymbol{v}^-$, $\boldsymbol{a}$ and $\boldsymbol{b}$ are column vectors and their elements are respectively v_l^+, v_l^-, a_{im} , and b_{im}. $\boldsymbol{\rho}$, $\boldsymbol{r}$, $\boldsymbol{t}$, and $\boldsymbol{s}$ are respectively the device reflection, reception, transmission and scattering matrices [9]. Additionally, the far-field pattern can be analytically obtained by means of the following expression

$$\boldsymbol{E}(\theta, \varphi) = \boldsymbol{etv}^+ \tag{4}$$

where $\boldsymbol{e}$ is a row vector of the transversal electric field component of the spherical modes. From (2), the expression of $\boldsymbol{Y}$ as a function of $\boldsymbol{S}$ can be readily obtained.

C. Axis rotation and coordinate origin change for GSM

The rotation of the reference axes and the change of origin of coordinates of the spherical ports allow us to choose the same coordinate system for all the convex spherical ports of each domain, so that all of them can be referred to a single spherical port that contains all of these domains. It can be carried out by means of a general translation matrix $\boldsymbol{G}_{jk}^{(2)}$ which relates complex amplitudes of incoming spherical modes between two spherical ports, *j* and *k*, and complex amplitudes of scattered spherical modes between the same two ports

$$\boldsymbol{b}_j^s = \boldsymbol{G}_{jk}^{(2)}\boldsymbol{b}_k^s \; ; \; \boldsymbol{a}_k = \left(\boldsymbol{G}_{jk}^{(2)}\right)^H \boldsymbol{a}_j \tag{5}$$

where

$$\boldsymbol{b}_j^s = \boldsymbol{b}_j - \boldsymbol{a}_j \tag{6}$$

and port *k* must be completely surrounded by port *j*. Matrix $\boldsymbol{G}_{jk}^{(2)}$ can be analytically built as explained in [6] but with the axial translation coefficients corresponding to the second case given in Appendix 3 of [9] (denoted here as $^{(2)}$), or in [10].

From (5) and (3) the submatrices of the GSM_C, with only one common spherical port *j*, can be computed from the submatrices of the GSM_G with, in general, multiple local spherical ports *k* through the following expressions:

$$\begin{aligned} &\boldsymbol{\rho}_C = \boldsymbol{\rho}_G \; ; \; \boldsymbol{t}_C = \boldsymbol{G}^{(2)}\boldsymbol{t}_G \\ &\boldsymbol{r}_C = \boldsymbol{r}_G\left(\boldsymbol{G}^{(2)}\right)^H \; ; \; \boldsymbol{s}_C = \boldsymbol{G}^{(2)}(\boldsymbol{s}_C - \boldsymbol{I})\left(\boldsymbol{G}^{(2)}\right)^H + \boldsymbol{I} \\ &\boldsymbol{G}^{(2)} = \left[\boldsymbol{G}_{j1}^{(2)} \; \boldsymbol{G}_{j2}^{(2)} \; \ldots \; \boldsymbol{G}_{jk}^{(2)}\right] \end{aligned} \tag{7}$$

with the superscript *H* denoting the conjugate transpose.

III. RESULTS

A. Beam-steerable, lens-based antenna system

Fig. 1 shows the structure under analysis and its geometrical description. It consists of a dielectric lens (ε_r = 2.35), [2], scaled to work at 19GHz. The lens can rotate around the y-axis, for $\theta_{steering} \in [0°, 40°]$. The DD proposed in this work is also shown in Fig. 1. Domain 1, D1, includes the lens and two spherical ports: the outer one to account for the radiating fields; the concave, inner one to host Domain 2, D2. Domain 2 includes the horn (fed by a circular waveguide port), covered by a CxSp. Both domains are FEM-solved independently, obtaining GAM_1 and GAM_2, respectively. By connecting GAM_1 and GAM_2 (when the outer CxSp of Domain 2 fits the inner CvSp of Domain 1), GAM_T arises containing the EM behavior of the complete structure. Fig. 2 shows results from this direct connection to verify the proposed FEM-DirectDD without rotation/translations (i.e. case $\theta_{steering}$ =0°). Results from only full-FEM and from this work show differences below 0.1 dB for E-field Right-/Left-Handed Circular Polarization (RHCP, LHCP). Therefore, the convex-to-concave connection is verified. From Table I, computational time for the proposed method is seen to be of the same order of magnitude as that from software in [11]. The advantages of

using the proposed method come now thanks to the fact that the GSM_2 can be analytically manipulated to obtain the GSM of the horn antenna rotated a defined angle $\theta_{steering}$, say $GSM'_{2,\theta}$ (where ' highlights the fact of being analytically computed). Next, by analytical connections of GAM_1 with every $GAM'_{2,\theta}$, it is obtained the EM behavior of the complete structure for any $\theta_{steering}$ within only 1-2 seconds per $\theta_{steering}$ value (as opposed to the 51min needed by [11]).

Results for $\theta_{steering}$ =10°, 40° are also shown in Fig. 2 to prove the accuracy of the proposed FEM-DirectDD technique when rotation is analytically applied. Discrepancies between this work and results from [11] are within the usual range observed when two numerical methods are compared (in this case, FEM in [11] also applied Integral Equation Boundary Conditions over the lens and absorbing boundary conditions). Up to 880 spherical modes where considered for the connection. Other advantages of the proposed technique will be highlighted thanks to the next example.

B. Small-satellite Fuselage Bread-Board

Fig. 3 shows a representative breadboard of the main features that small- and microsatellites may exhibit. The considered frequency band is 700-850MHz (42 frequency points), which is also representative of the working frequency of some units on-board (such as the TT&C [1]) and payload instruments [12]. The main fuselage has the shape of a truncated cone to proof that the proposed method also works whenever a hemi-sphere surface can be laid on a circumference. The radii of the bottom and upper bases are, respectively, 2300 mm and 1150 mm. The height is 800 mm. On the upper, circular base, three elements will be placed on positions ($\boldsymbol{r}_{A1}$, α_{A1}; $\boldsymbol{r}_{A2,}$ α_{A2} ; $\boldsymbol{r}_{P,}$ α_P) not specified *a priori*: two patch antennas (180mm×180mm), described by a single GAM_A; and a prism, metallic, passive element (99mm×99mm×130 mm), described by GAM_P. These three elements will be placed in 120°-circular rotation configuration on the upper base. A fourth element (a metallic cylinder, 250 mm in height) will be located near the base edge, see Fig. 3. This configuration allows to proof:

- The formulation works for both spherical ports and hemispherical ports laying on a metallic circumference.
- Replication of elements can be analytically done.
- Analytical rotations/translation can be used to set the desired position of any element, characterized by its GAM, inside a hemi-sphere (as long as no collision between spherical surfaces takes place).
- *Analytical domains* can be created.
- Domains –either analytically or FEM computed- can be nested inside each other.

The geometry is decomposed into the three different domains depicted as D1, D2, and D3. The radii of the outer-most spherical ports are, respectively (mm): 1500, 750, 500. As can be seen, Domain 3 (D3) is a so-defined analytical domain, and will host GSM_A (analytically operated to obtain 2 replications at different positions/rotations) and GSM_P.

Hence, following the procedure in Section II, GAM_{D1}, GAM_{D2}, GAM_A, and GAM_P from (respectively) D1, D2, the patch antenna, and the metallic scatter were computed by FEM (for these two latter, the radius of the outer-most, convex, hemispherical port is 180 mm). Then, $GSM_{G,D3}$ for Domain 3 is obtained from GSM_A by setting its desired position/rotation on the satellite ($\boldsymbol{r}_{A1}$, α_{A1}; $\boldsymbol{r}_{A2}$, α_{A2}); and from GSM_P, analytically placed at ($\boldsymbol{r}_P$,α_P). Then, $GSM_{C,D3}$ is computed and, from it, GAM_{D3}. Next, connection of GAM_{D3} and GAM_{D2} is performed, yielding GAM_{D23}; and, after connection with GAM_{D1}, the EM response of the complete structure is achieved. The computational details are given in Table II. We see that the FEM problems are carried out only once. However, since the position and the local rotation of each element, ($\boldsymbol{r}_i$, α_i), is set analytically, a large set of locations, along with their complete EM behaviors, can be assessed within 1-2 seconds each, as opposed to the 120min needed for the computation of the total geometry by [3].

In addition, the proposed technique allows to quickly evaluate the impact on EM performance in case an evolution of the fuselage happens (in our case-example, only D2 and/or D1 should be FEM-recomputed). Also, the redesign or the inclusion of other elements within Domain 3 can be assessed straightforward. So, a sizeable reduction in total computational time within the satellite design loop can be obtained, as shown in Table II.

Fig. 4 shows that the results obtained by the proposed technique are similar to that obtained by using FEM on the complete geometry ("Total" in Table II) for the 42 frequencies.

IV. Conclusion

As stated in the introduction, a hybrid FEM-DirectDD technique has been presented that allows relevant features in the space field, both on-ground and in-orbit. The implementation of the method has shown accuracy, robustness and efficiency. Most features of this technique have been successfully applied to breadboards of both lens-based antennas for satcoms, and small satellites. The former example allowed us to verify the accuracy and the computational time for connections and rotations; the latter demonstrated other useful advantages such as translation/rotation, replication, and nesting, which make the proposed technique (fully implemented as a general purpose tool) an efficient tool.

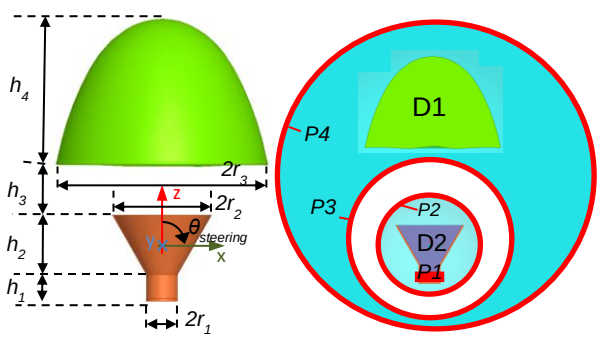

Fig. 1. General sketch of a lens-based antenna structure. In this work: r_1= 5.52mm; r_2= 19.65mm; r_3= 40mm; h_1= 10mm; h_2= 25mm; h_3= 22mm; h_4= 60mm. DirectDD applied:: D2, contains {*P1*: circular port; *P2*: CxSp, r=30 mm}; D1, contains { *P3*: CvSp, r=30 mm; *P4*: CxSp, r=70 mm}.

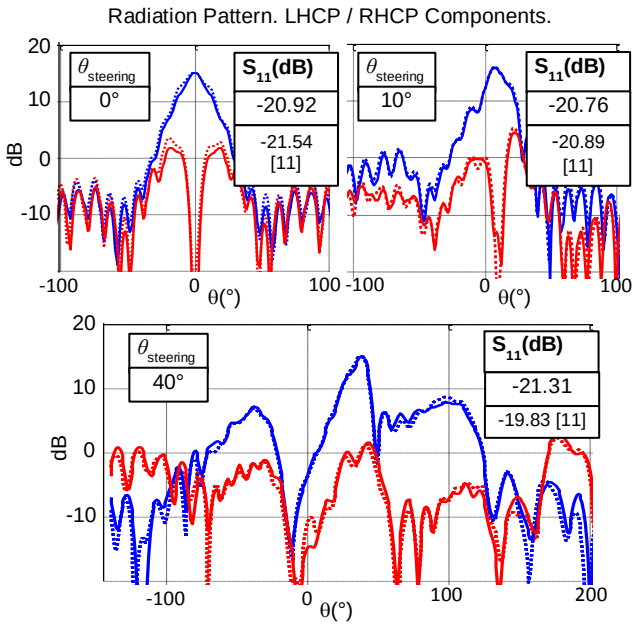

Fig. 2. Amplitude (dB) of RHCP (blue) and LHCP (red), at plane φ=0°, 19 GHz. a) Dot: FEM in [3]. b) Solid: this work. c) Dash: FEM-IE from [11]. NOTE: (a) and (b) are almost superimposed. Inset: S_{11}.

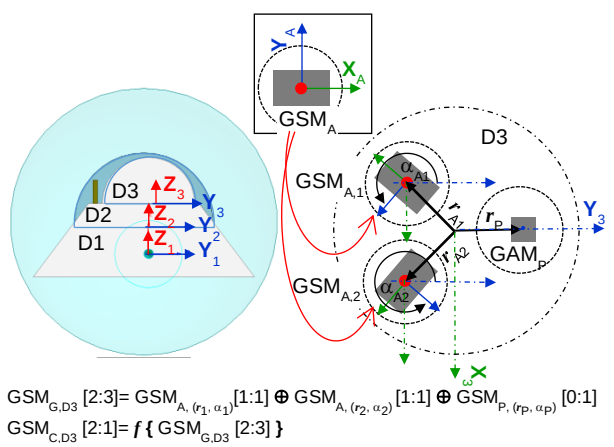

Fig. 3. Left: Cross section of the conical small-satellite fuselage bread-board. The geometry is devided into domains: D1, D2, D3. Right: Conceptual sketch of the analitical generation of $GSM_{C,D3}$. Beside each matrix name, the number of WGp, *n*, and CxSp, *m*, of each matrix: [*n*:*m*].

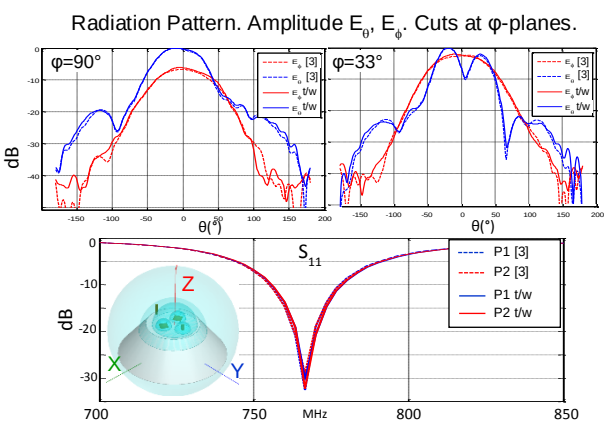

Fig. 4. Up: Amplitude (dB) of E_φ and E_θ. Cut at φ-planes with respect to the XYZ reference system shown. Down: S_{11} of Patch antennas P1, P2. Dash: EM simulation of complete geometry, [3]; Solid: this work, t/w.

TABLE I: COMPUTATIONAL DETAILS, 24-CORE 3.33 GHZ

	FEM	This work: D1/D2		FEM in [11]
# elem./ RAM (GB)	302K / 101	152K/115	105K/15	101K/16
CPU t	~90 min	~110min	~10 min	~51 min
# modes	*P1:2*	*P3:880*	*P1:2*	*P1: 2*
	P4:2176	*P4:2176*	*P2:880*	

TABLE II: COMPUTATIONAL DETAILS, 24-CORE 3.33 GHZ

	Total by[3]	This work: D1/D2/D3			Patch Ant.	Prism
# elem.	94K	45K	42K	-	32K	13K
RAM GB	14	7.4	4.7	-	1.5	1
CPU t (min)	~120	~43	~19	-	7	6
# modes:						
WGp	*2*				*2*	
CvSp		*576*	*576*			-
CxSp		*864*	*576*	*576*	*35*	*35*

REFERENCES

[1] T. Debogović, P. Robustillo, N. F. Bongard, M. Sabbadini , F. Tiezzi, J. R. Mosig, "Low-profile multi-function antenna system for small satellites," in *Proc. 10th EuCAP, Davos, Switzerland*, 2016. 10.1109/EuCAP.2016.7481858.

[2] J. S. Silva, E. B. Lima, J. R. Costa, C. A. Fernandes, J. R. Mosig, "Tx-Rx Lens-Based Satellite-on-the-Move Ka-Band Antenna," *IEEE Ant. and Wireless Prop. Letters*, vol.: 14, pp. 1408 – 1411, March 2015.

[3] J. Rubio, J. Arroyo, J. Zapata, "Analysis of passive microwave circuits by using a hybrid 2-D and 3-D finite-element mode-matching method," *IEEE Transactions on Microwave Theory and Techniques*, vol.:47, is. 9, pp. 1746-1749, Sept, 1999. 10.1109/TMTT.1999.788507.

[4] A. Barka, P. Caudrillier, "Domain Decomposition Method Based on Generalized Scattering Matrix for Installed Performance of Antennas on Aircraft," *IEEE Trans. Antennas Propag* vol. 55, no. 6, pp. 1833-1842, June 2007.

[5] C. Della Giovampaola, E. Martini, A. Toccafondi, S. Maci, Fellow, "A Hybrid PO/Generalized-Scattering-Matrix Approach for Estimating the Reflector Induced Mismatch," *IEEE Trans. Antennas Propag* , vol. 60, no. 9, pp. 4316-4325, Sept. 2012.

[6] J. Rubio, M. A. González, and J. Zapata, "Generalized-scattering-matrix analysis of a class of finite arrays of coupled antennas by using 3-D FEM and spherical mode expansion," *IEEE Trans. Antennas Propag.*, vol. 53, pp. 1133–1144, Mar. 2005.

[7] J. Rubio, M.A. Gonzalez, J. Zapata, A. Montesano, F. Monjas, L.E. Cuesta, "Full-wave analysis of the Galileo system navigation antenna by means of the generalized scattering matrix of a finite array," in *Proc. 1st EuCAP*, Nice, France, 2006. 10.1109/EUCAP.2006.4584554.

[8] *Waveguide Handbook*, ser. IEE Electromagnetic Waves Series, No 21. N. Marcuvitz. London, U.K.: Peter Peregrinus Ltd.,1986.

[9] J. E. Hansen, *Spherical Near Field Antenna Measurements*. Peter Peregrinus Ltd., London, U.K., 1988, pp. 47-48.

[10] I. P. Kovalyov, N. I. Kuzikova, D. M. Ponomarev, "Transformation of Antenna Generalized Scattering Matrix During Rotation and Linear Displacement," *IEEE Trans. Antennas Propag.*, vol.: 64 , is.: 12, pp. 5110 – 5121, Dec. 2016.

[11] HFSS©, ANSYS, http://www.ansys.com/

[12] Argos CNES, http://www.argos-system.org/